THE JOURNAL OF BIOLOGICAL CHEMISTRY
Vol. 273, No. 29, Issue of July 17, pp. 18429–18434, 1998
Printed in U.S.A.

Cryoelectron Microscopy and Image Analysis of the Cardiac Ryanodine Receptor*

(Received for publication, February 19, 1998, and in revised form, April 16, 1998)

Manjuli Rani Sharma‡§, Pawel Penczek‡¶, Robert Grassucci‡, Hong-Bo Xin‖, Sidney Fleischer‖, and Terence Wagenknecht‡**

*From the ‡Wadsworth Center for Laboratories and Research, New York State Department of Health, Albany, New York 12201-0509, the **Department of Biomedical Sciences, School of Public Health, State University of New York, Albany, New York 12222, and the ‖Department of Molecular Biology, Vanderbilt University, Nashville, Tennessee 37235*

The three-dimensional structure of the cardiac muscle ryanodine receptor (RyR2) is described and compared with its skeletal muscle isoform (RyR1). Previously, structural studies of RyR2 have not been as informative as those for RyR1 because optimal conditions for electron microscopy, which require low levels of phospholipid, are destabilizing for RyR2. A simple procedure was devised for diluting RyR2 (in phospholipid-containing buffer) into a lipid-free buffer directly on the electron microscope grid, followed by freezing within a few seconds. Cryoelectron microscopy of RyR2 so prepared yielded images of sufficient quality for analysis by single particle image processing. Averaged projection images for RyR2, as well as for RyR1, prepared under the same conditions, were found to be nearly identical in overall dimensions and appearance at the resolution attained, ≈30 Å. An initial three-dimensional reconstruction of RyR2 was determined (resolution ≈41 Å) and compared with previously reported reconstructions of RyR1. Although they looked similar, which is consistent with the similarity found for the projection images, and with expectations based on the 66% amino acid sequence identity of the two isoforms, structural differences near the corners of the cytoplasmic assembly were observed in both two- and three-dimensional studies.

Ryanodine receptors (RyRs)[1] are the major calcium release channels associated with the sarcoplasmic reticulum in striated muscle (for recent, reviews, see Refs. 1–5), and they are the largest ion channels known. The major receptor isoforms from skeletal (RyR1) and heart (RyR2) muscle are composed of four copies of a very large protein subunit (565 kDa) that has 66% amino acid sequence homology between the two isoforms. In addition to the large subunit, RyR1 and RyR2 are each associated with much smaller (12 kDa), isoform-specific modulatory polypeptides, also present in four copies per receptor, which have been identified as FK506-binding proteins (6–8). A third RyR isoform, RyR3, is expressed in a wide range of tissues, including mammalian brain and skeletal muscle. In fact, all three isoforms are expressed in multiple cell types.

In both skeletal and cardiac muscle, RyRs are thought to play a central role in excitation-contraction coupling by releasing Ca^{2+} into the myoplasm, and by mediating signal transduction between the plasma membrane/transverse- (T) tubule system and the sarcoplasmic reticulum. Dihydropyridine receptors (DHPRs), which are membrane-spanning voltage sensors in the plasma membrane/t-tubule system, communicate with the RyRs in the apposing junctional face membrane of the sarcoplasmic reticulum. Together, the RyRs and DHPRs are thought to form the major components of the signal transducing apparatus of excitation-contraction coupling. RyRs are present at specialized regions of the sarcoplasmic reticulum, the junctional face membranes of the terminal cisternae, which are closely apposed to the t-tubule. RyRs possess large cytoplasmic assemblies that span the ≈12 nm gap between the two membrane systems and had been visualized in electron micrographs of thin-sectioned muscle (9) long before their identification as RyRs (10–12).

As for the RyR, different isoforms of the DHPR are also present in heart and skeletal muscle, and current evidence suggests that the DHPR and RyR together are responsible for the different mechanisms of E-C coupling in the two types of muscle (13, 14). In skeletal muscle, DHPRs are thought to be physically coupled to RyRs and control their activity by a conformational coupling mechanism. In contrast, cardiac DHPRs function as voltage-regulated Ca^{2+} channels that control RyR activity by a Ca^{2+}-induced Ca^{2+} release mechanism.

Several lines of evidence have shown that the single channel properties of RyR1 and RyR2 that have been incorporated into lipid bilayers are similar but not identical. For example, differences are present between the two isoforms regarding their sensitivities to Ca^{2+} activation/inactivation and Mg^{2+} inhibition (15).

To help understand the different mechanisms of E-C coupling it is essential to characterize the structural differences of the two RyR isoforms, as well as those of the DHPR, and to relate these differences to functional consequences. With regard to the RyR, the overall sequence identity of RyR1 and RyR2 is 66% (16–20), but three subregions show much less homology and are, therefore, likely to be responsible for the functional differences of the two isoforms. Mutagenesis of these regions together with functional expression in cultured myocytes will clarify which regions are responsible for the different properties of RyR1 and RyR2 (14).

The three-dimensional architecture of solubilized RyR1 has been investigated by cryoelectron microscopy and single-parti-

* This work was supported in part by National Institutes of Health Grants AR40615 (to T. W.) and HL32711 and the Muscular Dystrophy Association (to S. F). The costs of publication of this article were defrayed in part by the payment of page charges. This article must therefore be hereby marked "*advertisement*" in accordance with 18 U.S.C. Section 1734 solely to indicate this fact.

§ Recipient of American Heart Association Fellowship 960124. To whom all correspondence should be addressed.

¶ Supported by National Institutes of Health Grant GM29169 (Joachim Frank).

[1] The abbreviations used are: RyR, ryanodine receptor; RyR1, skeletal muscle ryanodine receptors; RyR2, cardiac muscle ryanodine receptors; E-C coupling, excitation-contraction coupling; DHPR, dihydropyridine receptor; SBL, soybean phospholipid; CHAPS, 3-[3-cholamidopropyl)dimethylammonio]-1-propanesulfonic acid.

cle image processing methods (21–28, 31). Although the resolution of such studies has been limited to 30–40 Å, numerous structural details have been resolved for RyR1, and for RyR1 complexed with some of the proteins with which it interacts *in vivo* (25).

To further understand the structural basis of the differing mechanisms of E-C coupling in heart and skeletal muscle, we have attempted to characterize RyR2 by electron microscopy. Until recently these studies have been unsuccessful owing to structural instability of RyR2 as compared with RyR1. Here we describe a procedure for imaging of RyR2 by cryoelectron microscopy, and provide the first three-dimensional reconstruction of RyR2.

MATERIALS AND METHODS

Preparation of RyRs—Cardiac RyR2s were purified from dog heart ventricles (12) by sucrose density gradient centrifugation (10, 29). The pooled peak fractions containing RyR2 were in a buffer containing 0.02 M Tris-HCl (pH 7.4), 1 M NaCl, 2 mM dithiothreitol, 4 μg/ml leupeptin, 0.5% CHAPS, 0.25% soybean phospholipid (SBL), and ≈20% sucrose. For optimal electron microscopy it was necessary to concentrate the receptor, which was accomplished by adsorption to heparin-agarose (11) at reduced NaCl (0.2 M, which was attained by dilution of the pooled peak fractions into NaCl-free buffer), followed by elution into the gradient buffer supplemented with 1.0 μg/ml pepstatin, 100 μM phenylmethylsulfonyl fluoride, and lacking sucrose (buffer A). RyR1 was purified from rabbit skeletal muscle as described previously (10, 25, 29), and the final buffer was modified to contain 1% CHAPS and 0.5% SBL.

Preparation of Grids for Cryoelectron Microscopy—The following procedure was followed for collecting the microscopy data used to determine the two-dimensional projection averages. RyR2 in buffer A was diluted so that the final concentrations of CHAPS and SBL were 0.5% (w/v) and 0.25% (w/v), respectively, and EGTA was present at 1 mM to maintain the receptor in a closed state. All other buffer components were the same as for buffer A. To avoid prolonged exposure to lipid-free conditions, 0.5 μl of RyR2 (0.25–0.50 mg/ml) was diluted 10-fold into 4.5 μl of buffer B (same as buffer A except that SBL was absent), on the grid. The grid was then immediately rinsed by holding the specimen side on a drop of buffer C (same as buffer A, except that no SBL was present and [CHAPS] = 0.5%). For purposes of comparison, grids of RyR1 were prepared using the identical procedure. The procedure employed for obtaining the data used for computing the three-dimensional image reconstruction differed by the absence of EGTA in the buffers.

Cryoelectron Microscopy—Grids were transferred while under liquid nitrogen to a Gatan (model 626) cryoholder. Micrographs were recorded with the objective lens underfocussed by 1.8–2.0 μm at a nominal magnification of 38,000 × and with a net electron dose estimated at 10 e^{-}/Å^2, using a Philips EM420 transmission electron microscope equipped with a goniometer stage and low dose kit, and operated at 100 kV. Specimen temperatures were maintained at −176 ± 2 °C.

Image Processing—The suitability of the micrographs for image processing was checked by optical diffraction for image defects (astigmatism, specimen charging, and drift) and appropriate defocus (31). Selected micrographs were digitized using a Perkin-Elmer PDS 1010A flatbed scanning microdensitometer (Orbital Sciences, Pomona, CA) with a step size of 20 μm corresponding to 5.3 Å on the object scale. The SPIDER software package (30) was used for all image processing. The procedures used for averaging images of receptors in the 4-fold symmetric orientation and for determining difference images have been previously described (23, 31).

It was found that micrographs of RyR2 contain images of apparently well preserved receptors in many different orientations, thereby obviating the requirement of tilting the specimen grid (37, 38). RyR1 in the present experimental conditions shows a strong propensity for the orientations displaying 4-fold symmetry and would require tilting the specimen grid to determine a three-dimensional reconstruction, in agreement with our earlier structural analysis of RyR1. Therefore, for RyR2 we employed a method of three-dimensional reconstruction applicable to macromolecules that display multiple orientations on the specimen grid that was developed by Penczek *et al.* (32). In this method, experimental images of the macromolecule are matched to images that are computed by projecting a pre-existing three-dimensional model over a sampling of all possible orientations, and a three-dimensional reconstruction is determined from the experimental images based upon the assigned viewing directions. By iterating the procedure using the output of the previous iteration as the input model for the current one, any bias caused by the initial model is reduced.

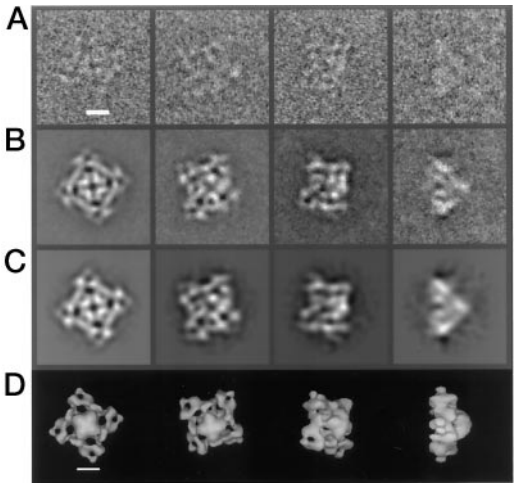

FIG. 1. **Evaluation of three-dimensional reconstruction algorithm performance.** *A*, selected experimental images representing 4 of the 48 evenly spaced orientations obtained from the starting model (see "Materials and Methods" for details). *B*, images obtained by averaging all of the experimental images that were assigned to the same 4 orientations. *C,* projection images computed from the final three-dimensional reconstruction of RyR2. Note similarity to the averaged experimental images in *C*. *D*, solid-body representations of the three-dimensional reconstruction of RyR2 in the orientations that produce the images shown in *C* when projected along a normal to the plane of the figure. *Scale bar*, 100 Å.

We have applied this algorithm to micrographs of frozen hydrated RyR2 using a previous reconstruction of RyR1 as the starting model (31). This starting model was thus used as template structure to compute 48 reference projections so as to cover the entire angular space evenly. Initially, a set of 4,143 images of individual receptors ("experimental projections," *e.g.* see Fig. 1*A*) were cross-correlated with this reference set of 48 quasi-evenly spaced projections. This was done to classify the total number of orientations present in the complete experimental data set. The projection angles of the experimental projections were assigned as those corresponding to the reference projection yielding the highest cross-correlation coefficient. Those images showing the highest correlation with the reference projections were retained for further consideration and refinement of orientation parameters. From these images an initial reconstruction was computed which used 1264 reference projections derived from the starting model. Subsequent iterations were correlated with 1264 projections derived from current reconstruction of RyR2. As a check on the success of the orientational assignments, experimental projection images that were assigned to a given reference projection were rotationally and translationally aligned to one another so that an averaged image could be computed (*e.g.* Fig. 1*B*) and compared with the matching projection computed from the final three-dimensional reconstruction (*e.g.* Fig. 1*C*). The final reconstruction was computed from 600 particle images, and additional averaging was attained by enforcing 4-fold symmetry. To display the three-dimensional reconstruction of RyR2, a threshold was chosen as described previously (31). The final resolution was estimated by Fourier shell correlation with the cut-off value of 0.5 (33). A nominal resolution of 41 Å was obtained.

RESULTS AND DISCUSSION

Electron Microscopy of RyR2—Initial attempts to image RyR2 by cryoelectron microscopy using the same procedures as were employed previously for RyR1 (21–23) were unsuccessful; nearly all of the RyR2 complexes appeared to be distorted or aggregated (Fig. 1*A*), and few images displaying the expected 4-fold symmetry were apparent. For these studies the receptors were isolated in a buffer containing detergent (0.5–1.0% CHAPS), but lacking phospholipid. Similar results by the negative staining technique have been reported (34). Since earlier studies demonstrated an irreversible loss in ryanodine binding activity upon removal of phospholipid from purified RyR2 (12, 35), we surmised that the omission of lipids might be respon-

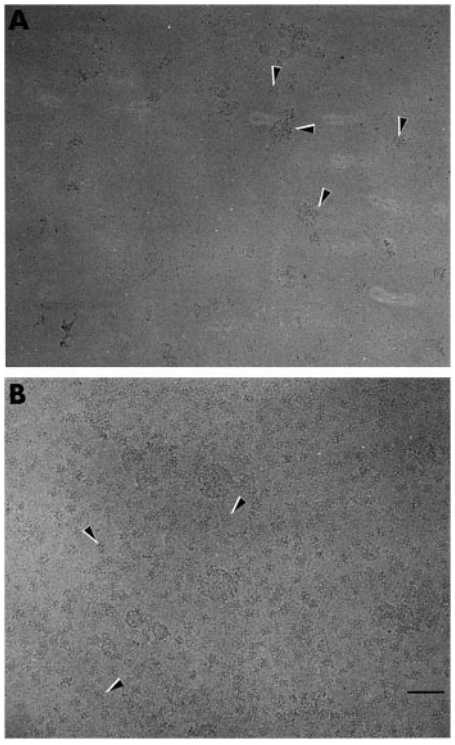

FIG. 2. **Cryoelectron microscopy of cardiac RyR2.** Portions of micrograph recorded with the specimen grid not tilted. *A*, micrograph of RyR2 prepared in the absence of lipids showing aggregates (*arrow*) and image of distorted receptors. *B,* cryoelectron micrograph of well preserved cardiac channels prepared in the presence of phospholipids and diluted into lipid-free buffer (see "Materials and Methods"). A few of the particles are marked with *arrows*. Scale bar, 1000 Å.

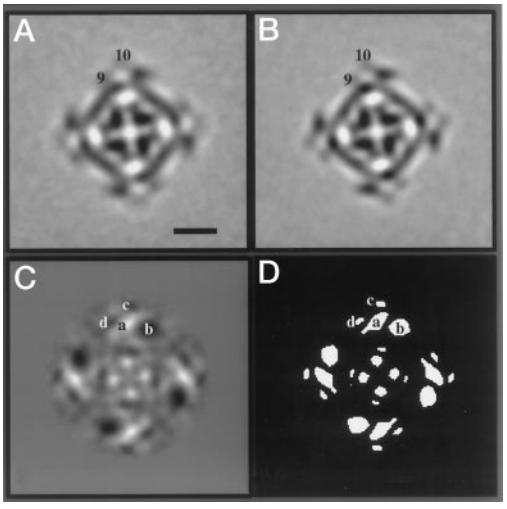

FIG. 3. **Averaged images of cardiac and skeletal muscle ryanodine receptors (RyR2 and RyR1) in one of the two 4-fold symmetric orientations (face-up).** *A*, average of RyR2 ($n = 231$). *B*, average RyR1 ($n = 232$). *C*, difference image obtained by subtracting image B from image A. The main differences at outer radii are indicated by *a, b, c,* and *d. D,* map of statistically significant differences (shown in *white*), which correspond to regions where the differences shown in *C* exceed the standard error of the difference by a factor of 3 or more, corresponding to significance level of $p = 98\%$ (see Ref. 41). *Scale bar*, 100 Å.

sible for the apparent loss in structural integrity. However, phospholipid at the levels commonly employed in the purification of RyR2, 2.5–5 mg/ml, interferes with cryoelectron microscopy by reducing the contrast to unacceptably low levels.

To address this problem we tried isolating RyR2 in the presence of phospholipid and removing the latter just before electron microscopy by adsorbing the receptors onto heparin-agarose, and then eluting them into lipid-free buffer. We also tested the effect of diluting concentrated RyR2 in the presence of phospholipid into lipid-free buffer within minutes of applying the sample to electron microscopy grids. Neither of these approaches increased substantially the frequency of images of structurally intact receptors. Last, we tried diluting (10–20-fold) RyR2 in phospholipid containing buffer directly onto a carbon-coated specimen grid to which lipid-free buffer had been previously applied, followed within seconds by rinsing, blotting, and freezing (see "Materials and Methods" for details). By this procedure we obtained a marked increase in the frequency of isolated (*i.e.* non-aggregated) RyR2 complexes and also of the distinctive 4-fold symmetric images (Fig. 2*B*). The contrast of RyR2 in these micrographs was still somewhat reduced, due to the presence of residual lipids, as compared with images of skeletal muscle receptors observed previously (31), but, as shown above, the images of RyR2 were suitable for application of single-particle image processing techniques.

Two-dimensional Image Analysis of RyR2—Images of frozen hydrated RyR2s in the 4-fold symmetric orientation were selected from micrographs such as that shown in Fig. 2*B*, and the particles were aligned by correlation methods. The aligned images were subjected to correspondence analysis and classification techniques, and two principal classes of roughly equal numbers were identified which correspond to receptors lying either face up or face down on the carbon support surface of the microscope grid. The same behavior has been observed previously for RyR1 (31). Averages of the aligned and classified RyR2 for each of the two classes were computed, and one of them is shown in Fig. 3*A*. The face-up and face-down averages, which show the three-dimensional density distribution of the receptor projected along opposing directions of the 4-fold symmetry axis, are simply mirror images of each other, and are otherwise essentially identical. The reproducibility of the averaged images extended to 32 Å as assessed by the Fourier ring-correlation method (33, 36).

To aid in comparing the structures of RyR2 and RyR1, we also determined averages of RyR1 in parallel using the same buffer and imaging conditions as were used for RyR2. For this study, EGTA (1 mM) was included in the buffers to ensure that the receptors are in the closed state (28). Examination of averaged RyR2 and RyR1 images shows that they are very similar (Fig. 3, *A* and *B*, respectively), which is not surprising given the high sequence homology of the two proteins (16–20). Both are square in overall shape with an edge length of 280–290 Å, and show the same complex pattern of density distribution that has been observed previously for RyR1 (22, 31). The three-dimensional architecture of RyR1 is known to a resolution of ~30 Å, and based upon the similarities of the average projected structures, some inferences about the three-dimensional architecture of RyR2 are justified. For example, all of the density outside the dense central region (radii greater than 75 Å) of the averaged RyR2 image arises from the cytoplasmic portion of the receptor. Density forming the central region of the averaged RyR2 contains contributions from both cytoplasmic and transmembrane regions of the receptor.

A difference image (Fig. 3*C*), formed by subtracting the RyR1 average (Fig. 3*B*) from the RyR2 image (Fig. 3*A*), shows some regions of both positive and negative differences in density between the two isoforms. Much of the statistically significant difference (Fig. 3*D*), in terms of area, is near the corners of the receptor (regions labeled "*a,*" "*b,*" "*c,*" and "*d*"). Three-dimensional reconstruction has shown that the corner regions, also referred to as "clamps," comprise a cluster of 5 or more domains in the cytoplasmic portion of the receptor (27, 31). Some smaller regions of difference are also apparent in Fig. 3*C* cor-

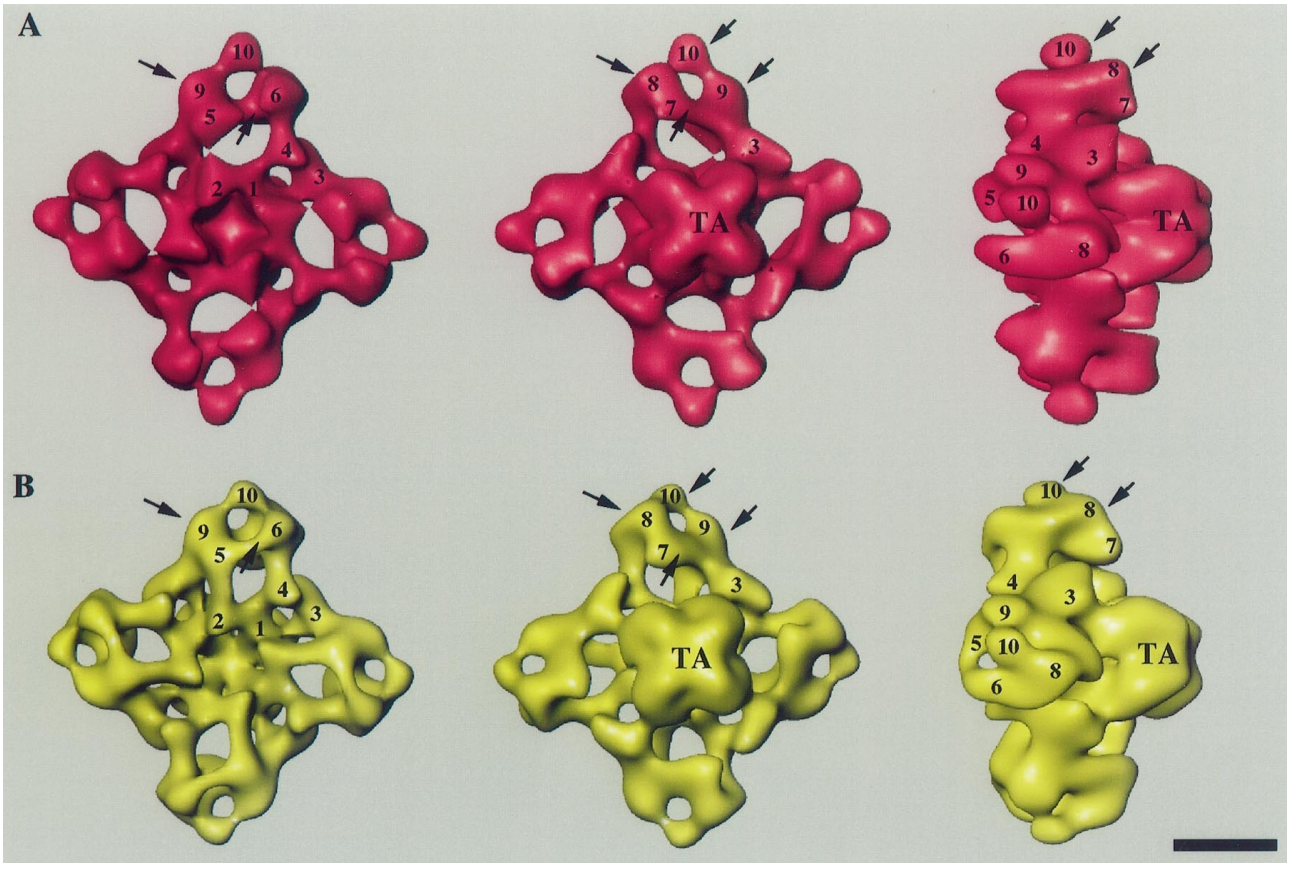

FIG. 4. **Three-dimensional surface representation of RyR2 (*A*) and comparison with RyR1 (*B*).** Leftmost vertical group of *A* and *B* shows the t-tubule face of the receptors along the 4-fold axis. This is the surface that would face the cytoplasm and the apposing transverse tubule in a dyad-triad junction. The *middle* group shows a view along the 4-fold axis onto the surface that would interact with the sarcoplasmic reticulum, and the rightmost group shows RyR2 and RyR1 in a side view (normal to 4-fold axis). *Arrows* point to obvious differences between RyR2 and RyR1. The putative structural domains are labeled with numerals *1–10*. *TA*, transmembrane assembly. *Scale bar,* 100 Å.

responding to the central regions of the averaged receptor images, and could correspond to differences in either the cytoplasmic or transmembrane regions of the receptor. An error analysis of the difference image indicated that the larger differences are of high statistical significance ($p < 0.001$). Two independent difference images showed similar distributions in the clamp regions of the receptors, but the differences at lower radii (<75 Å) showed more variability, and so we are more confident that the differences at high radii do indeed correspond to genuine structural differences between the two isoforms.

Three-dimensional Reconstruction—An initial reconstruction of RyR2 has been determined by a projection matching algorithm (32). The three-dimensional structure of RyR2 is shown in Fig. 4*A*, represented as a solid surface in three orientations. Corresponding views of RyR1 from previous work (31) are shown in Fig. 4*B*. Both reconstructions were low-pass filtered to match the limiting resolution of 41 Å obtained for RyR2, which is lower than was obtained for RyR1 (31). Probably the lower resolution of RyR2 is due to the lower signal-to-noise ratio of RyR2 resulting from the presence of residual lipids on the electron microscope grid, and by the paucity of non-4-fold symmetric views of RyR2 available for inclusion in the reconstruction. Improvements in the resolution of ryanodine receptor reconstructions by the projection matching technique (32) will likely require significantly larger data sets to compensate for these effects. Additionally, micrographs will have to be recorded at several values of objective lens defocus. Following this strategy, a resolution of about 15 Å has been attained for another non-crystalline macromolecular complex, the prokaryotic ribosome.[2]

The similarity of the RyR1 and RyR2 reconstructions is their most striking feature (Fig. 4). Both consist of a transmembrane assembly and a larger cytoplasmic assembly comprising multiple domains (numbered in Fig. 4), all of which are present in both isoforms. Again, this similarity is not surprising in view of the high degree of sequence conservation between RyR1 and RyR2 (18, 19).

Closer inspection of the reconstructions reveals some differences in the size or shape of certain domains (indicated by *arrows* in Fig. 4). In particular, differences appear in the corner (clamp) regions of the cytoplasmic assembly where domains 8, 9, and 10 appear somewhat larger, whereas domain 7 is somewhat smaller in RyR2 relative to RyR1. The region between domains 5 and 6 appears to be connected by a bridge of density in RyR1 (Fig. 4*B*, *left panel*) that is absent, or weaker, in RyR2 (*cf. left panels* of Fig. 4, *A* and *B*); however, this bridging density has been found to vary among reconstructions of RyR1, and so the significance of this difference is unclear (31). The detailed appearance of three-dimensional reconstructions represented as surfaces can be strongly dependent on the threshold chosen to represent them, and therefore we show in Fig. 5 the RyR1 and RyR2 reconstructions superimposed with the regions of greatest difference obtained by subtracting the two reconstructions. Fig. 5*A* shows the RyR1 reconstruction with differences attributable to extra density present in RyR2, and Fig. 5*B*

[2] J. Frank, personal communication.

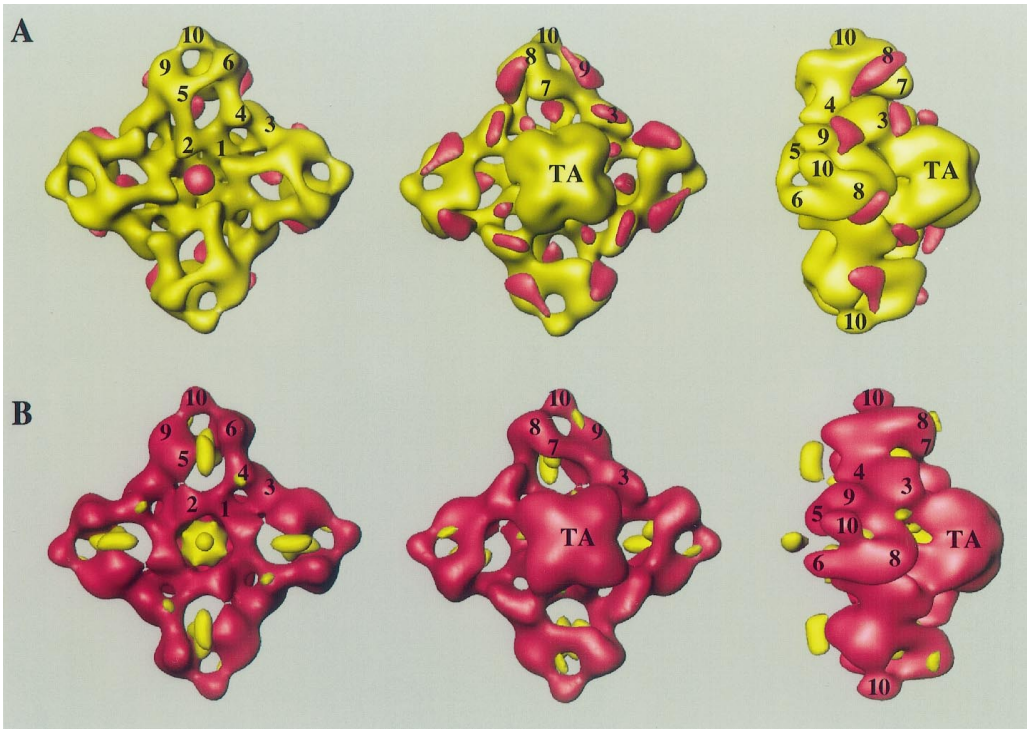

FIG. 5. **Differences between RyR1 and RyR2 from three-dimensional reconstructions.** The three-dimensional reconstructions were subtracted and contoured to show the largest differences in density between the two. *A*, the RyR1 reconstruction (*yellow*) is shown with the differences corresponding to extra density in RyR2 superposed in *rose*. *B*, the RyR2 reconstruction (*rose*) with the differences corresponding to excess density in RyR1 superposed in *yellow*.

shows RyR2 superimposed with differences corresponding to additional density in RyR1. Many of the differences that appear in the corner regions are consistent with the interpretations made above comparing RyR1 and RyR2 reconstructions directly; for example, the excess density that is present in RyR1 between domains 5 and 6 is a prominent feature of Fig. 5*B* (*left* and *right panels*), whereas domains 8 and 9 appear to contain more density in RyR2 (Fig. 5*A*, *middle panel*).

Unfortunately, it is difficult to assess the statistical significance of the differences observed for the three-dimensional reconstructions (39). However, as discussed above, an analysis of the statistical significance of the differences between the two-dimensional averaged projection images of RyR1 and RyR2 is feasible (Fig. 3*D*). In support of the significance of the differences between RyR1 and RyR2 in the clamps, it should be noted that they occur in the regions of the structure that also showed the largest differences in the averaged projection images discussed in the previous section. Furthermore, the regions within each clamp showing the greatest differences in the two-dimensional projection averages of RyR1 and RyR2 (in Fig. 3, *C*, *D* the regions labeled *a, b, c*, and *d*) correlate well, both in position and sign, with the differences in the three-dimensional reconstructions. For example, the region of difference labeled "*b*" in Fig. 3, *C* and *D* indicates an excess mass in RyR2 relative to RyR1; in the three-dimensional reconstructions the excess mass in domain 8 of RyR2 relative to RyR1 (Fig. 4, *far right panels*, and Fig. 5) lies in the region defined by region *b* in the two-dimensional difference map. Similarly, the extra density in RyR1 corresponding to the region between domains 5 and 6 (Figs. 4 and 5, *left panels*) and domain 7 (Figs. 4 and 5, *middle panels*) correlates in location with the region labeled *a* in the difference map of the averaged projections (Fig. 3*C*).

Interestingly, the clamp regions are thought to interact with the dihydropyridine receptor in skeletal muscle (25), and so differences in these regions may contribute to the differing mechanisms of excitation-contraction coupling in skeletal and cardiac muscle. Comparative analysis of the amino acid sequences of RyR isoforms has identified two highly divergent regions in the portion of the sequence that forms the cytoplasmic assembly (16, 40). Future studies employing sequence-specific probes in conjunction with three-dimensional reconstruction should allow unambiguous correlations of sequence and three-dimensional structure, which in turn should aid in understanding the functional differences observed for the RyR isoforms.

Acknowledgments—We thank Dr. Phillip Williams (Department of Surgery, Vanderbilt University Medical School) for supplying the canine hearts used in this study. We gratefully acknowledge the use and technical assistance of the Wadsworth Center's electron microscopy and image processing core facilities.

REFERENCES

1. Fleischer, S., and Inui, M. (1989) *Annu. Rev Biophys. Biophys. Chem.* **18,** 333–364
2. Franzini-Armstrong, C., and Protasi, F. (1997) *Physiol. Rev.* **77,** 699–729
3. Marks, A. R. (1997) *Am. J. Physiol.* **272,** H597—H605
4. Sutko, J. L., and Airey, J. A. (1996) *Physiol. Rev.* **76,** 1027–1071
5. Sorrentino, V., (1995) in *Ryanodine Receptors* (Sorrentino, V., ed) pp. 85–100, CRC Press, Boca Raton, FL
6. Jayaraman, T., Brillantes, A. M., Timerman, A. P., Fleischer, S., Erdjument-Bromage, H., Tempst, P., and Marks, A. R. (1992) *J. Biol. Chem.* **267,** 9474–9477
7. Lam, E., Martin, M. M., Timerman, A. P., Sabers, C., Fleischer, S., Lukas, T., Abraham, R. T., O'Keefe S. J., O'Neill, E. A., and Wiederrecht, G. J. (1995) *J. Biol. Chem.* **270,** 26511–26522
8. Timerman, A. P., Ogunbumni, E., Freund, E., Wiederrecht, G., Marks, A. R., and Fleischer, S. (1993) *J. Biol. Chem.* **268,** 22992–22999
9. Franzini-Armstrong, C. (1970) *J. Cell Biol.* **47,** 488–499
10. Lai, F. A., Erickson, H. P., Rousseau, E., Liu, Q. Y., and Meissner, G. (1988) *Nature* **331,** 315–319
11. Inui, M., Saito, A., and Fleischer, S. (1987) *J. Biol. Chem.* **262,** 1740–1747
12. Inui, M., Saito, A., and Fleischer, S. (1987) *J. Biol. Chem.* **262,** 15637–15642
13. Yamazawa, T., Takeshima, H., Sakurai, T., Endo, M., and Iino, M. (1996) *EMBO J.* **15,** 6172–6177
14. Yamazawa, T., Takeshima, H., Shimuta, M., and Iino, M. (1997) *J. Biol. Chem.* **272,** 8161–8164
15. Copello, J. A., Barg, S., Onove, H., and Fleischer, S. (1997) *Biophys. J.* **73,** 141–151
16. Takeshima, H., Nishimura, S., Matsumoto, T., Ishida, H., Kangawa, K., Minamino, N., Matsuo, H., Ueda, M., Hanaoka, M., Hirose, T., and Numa,

S. (1989) *Nature* **339,** 439–445
17. Zorzato, F., Fujii, J., Otsu, K., Phillips, M., Green, N. M., Lai, F. A., Meissner, G., and MacLennan, D. H. (1990) *J. Biol. Chem.* **265,** 2244–2256
18. Otsu, K., Willard, H. F., Khanna, V. K., Zorzato, F., Green, N. M., and MacLennan, D. H. (1990) *J. Biol. Chem.* **265,** 13472–13483
19. Nakai, J., Imagawa, T., Hakamata, Y., Shigekawa, M., Takeshima, H., and Numa, S. (1997) *FEBS Lett.* **271,** 169–177
20. Tunwell, R. E. A., Wickenden, C., Bertrand, B. M. A., Shevchenko, V. I., Walsh, M. B., Allen, P. D., and Lai, F. A. (1996) *Biochem. J.* **318,** 477–487
21. Wagenknecht, T., Grassucci, R., Frank, J., Saito, A., Inui, M., and Fleischer, S. (1989) *Nature* **338,** 167–170
22. Radermacher, M., Wagenknecht, T., Grassucci, R., Frank, J., Inui, M., Chadwick, C., and Fleischer, S. (1992) *Biophys. J.* **61,** 936–940
23. Wagenknecht, T., Berkowitz, J., Grassucci, R., Timerman, A. P., and Fleischer, S. (1994) *Biophys. J.* **67,** 2286–2295
24. Wagenknecht, T., and Radermacher, M. (1995) *FEBS Lett.* **369,** 43–46
25. Wagenknecht, T., Grassucci, R., Berkowitz, J., Wiederrecht, G. J., Xin, H-B., and Fleischer, S. (1996) *Biophys. J.* **70,** 1709–1715
26. Wagenknecht, T., and Radermacher, M. (1997) *Curr. Opin. Struct. Biol.* **7,** 258–265
27. Serysheva, II., Orlova, E. V., Chiu, W., Sherman, M. B., Hamilton, S. L., and van Heel, M. (1995) *Struct. Biol.* **2,** 18–24
28. Orlova, E. V., Serysheva, I. I., van Heel, M., Hamilton, S. L., and Chiu, W. (1996) *Nat. Struct. Biol.* **3,** 547–552
29. Timerman, A. P., Jayaraman, T., Wiederrecht, G., Onoue, H., Marks, A. R., and Fleischer, S. (1994) *Biochem. Biophys. Res. Commun.* **198,** 701–706
30. Frank, J., Radermacher, M., Penczek, P., Zhu, J., Li, Y., Ladjadj, M., and Leith, A. (1996) *J. Struct. Biol.* **116,** 190–199
31. Radermacher, M., Rao, V., Grassucci, R., Frank, J., Timerman, A. P., Fleischer, S., and Wagenknecht, T. (1994) *J. Cell Biol.* **127,** 411–423
32. Penczek, P. A., Grassucci, R. A., and Frank, J. (1994) *Ultramicroscopy* **53,** 251–270
33. Bottcher, B., Wynne, S. A., and Crowther, R. A. (1997) *Nature* **386,** 88–91
34. Anderson, K., Lai, F. A., Liu, Q. Y., Rousseau, E., Erickson, H. P., and Meissner, G. (1989) *J. Biol. Chem.* **264,** 1329–1335
35. Inui, M., and Fleischer, S. (1988) *Method Enzymol.* **157,** 490–505
36. Frank, J., Verschoor, A., and Boublik, M. (1981) *Science* **214,** 1353–1355
37. Radermacher, M., Wagenknecht, T., Verschoor, A., and Frank, J. (1987) *J. Microscop.* **146,** 113–136
38. Radermacher, M. (1988) *J. Electron Microscop. Tech.* **9,** 359–394
39. Liu W., amd Frank J. (1995) *J. Opt. Soc. Am.* **12,** A2615–2627
40. Sorrentino, V., and Volpe, P. (1993) *Trends Pharmacol. Sci.* **14,** 98–103
41. Frank, J. (1996) *Three-Dimensional Electron Microscopy of Macromolecular Assemblies,* Academic Press, San Diego, U. S. A.